



A Floating Small Target Identification Method Based on Doppler Time Series Information

Hengli Yu ¹, Hao Ding ^{1,*}, Zheng Cao ¹, Ningbo Liu ¹, Guoqing Wang ¹ and Zhaoxiang Zhang ²

¹ Marine Target Detection Research Group, Naval Aviation University, Yantai 246001, China; xdhenry@tom.com (H.Y.); caoziyuan0707@tom.com (Z.C.); lnb198300@sohu.com (N.L.); gqwang80@tom.com (G.W.)

² 92116 Troop, PLA, Huludao 125000, China; zzx1814255796@tom.com

* Correspondence: hao3431@tom.com; Tel.: +86-150-9848-7693

Abstract: Traditional radar detection methods heavily rely on the signal-to-clutter ratio (SCR); a variety of feature-based detection methods have been proposed, providing a new way for radar detection and the recognition of weak targets. Existing feature-based detection methods determine the presence or absence of a target based on whether the feature value is within the judgment region, generally focusing only on the distribution of features and making insufficient use of inter-feature chronological information. This paper uses the autoregressive (AR) model to model and predict the time sequence of radar echoes in the feature domain and takes the chronological information of historical frame features as the prior information to form new features for detection on this basis. A classification method for floating small targets based on the Doppler spectrum centroid sequence is proposed. By using the AR model to fit the Doppler spectrum centroid feature sequence of the target, the model coefficients are regarded as the secondary features for target identification. The measured data show that the correct classification and identification rate of this method for ship targets and floating small targets can reach over 92% by using 50 centroid features.

Keywords: radar detection; floating small target; autoregressive (AR) model; doppler spectrum centroid sequence; classification method



Citation: Yu, H.; Ding, H.; Cao, Z.; Liu, N.; Wang, G.; Zhang, Z. A Floating Small Target Identification Method Based on Doppler Time Series Information. *Remote Sens.* **2024**, *16*, 505. <https://doi.org/10.3390/rs16030505>

Academic Editors: Reza Shahidi and Eric Gill

Received: 14 November 2023

Revised: 5 January 2024

Accepted: 5 January 2024

Published: 28 January 2024



Copyright: © 2024 by the authors. Licensee MDPI, Basel, Switzerland. This article is an open access article distributed under the terms and conditions of the Creative Commons Attribution (CC BY) license (<https://creativecommons.org/licenses/by/4.0/>).

1. Introduction

Marine radar serves as a principal sensor for detecting maritime objects by processing the electromagnetic scattering echoes to identify and locate targets at sea; thus, studying the electromagnetic scatter reflections on the sea surface holds significant importance [1]. Currently, the objectives of studying the signals from radar electromagnetic scattering echoes off the sea surface are twofold: first, to extract marine environmental parameters such as wave height, wave direction, and wind direction from the sea echo signals, thereby discerning environmental background information through radar echoes; and second, to detect objects such as ships, channel buoys, and floating ice from the complex sea echo signals, where the maritime electromagnetic scatter reflection signals act as interference, commonly referred to as sea clutter [2]. The precise definition of sea clutter is the backscatter of radar-transmitted electromagnetic waves by the sea surface. The physical mechanisms forming sea clutter are highly complex and are influenced by various factors, including maritime environmental conditions, radar operational parameters, and radar working modes [3,4]. The main difficulties faced in the detection of weak targets within sea clutter are as follows: First, the complex characteristics of sea clutter make it challenging to model and suppress. With the proliferation and development of radars with high ranges and high Doppler resolutions (a “dual-high” system), the target is prone to diffusion in terms of distance and Doppler frequency; traditional models such as Gaussian distribution are no longer applicable. Sea clutter exhibits notable non-Gaussian, nonstationary, and non-homogeneous features, increasing the difficulty of understanding and suppressing clutter.

Under high-resolution, low-grazing angle, and high-sea state conditions, sea spikes are prone to occur, and the amplitude features of sea spikes and targets are extremely similar, resulting in a significant number of false alarms when utilizing energy domain detection methods. Second, establishing a target model is challenging. The interaction between maritime objects and the sea surface is complex, and due to the stochastic nature of sea motion, the movement of the targets also exhibits considerable randomness. The complex characteristics of target echoes make it difficult to describe all target echoes using a unified parameter model [5–8].

Feature detection methods represent an emerging category of radar target detection techniques, signifying a requisite transition toward the era of intelligent detection. On the one hand, these methods can effectively utilize the rich echo information provided by “dual-high” system radars, and on the other hand, they can transform the radar target detection problem into a classification problem, simplifying the complexity of target detection. Consequently, feature detection methods constitute an effective avenue for addressing the aforementioned issues [9,10]. Moreover, the approach to feature detection can also be applied to the identification of marine environmental background information, reducing the difficulty of extracting oceanic parameters such as wave height.

In 1993, LO T et al. first applied the single-scale fractal dimension for maritime target detection [11]. A single fractal parameter can only describe the fractal characteristics of the ensemble as a whole and is unable to reflect the details at different scales. To address this, Kaplan and others investigated the extended self-similar properties of fractional Brownian motion [12], seeking to improve the signal-to-clutter ratio in the time domain and enhance the distinction between sea clutter and target echoes in terms of fractal characteristics. Substantial research has been undertaken on the fractal properties of sea clutter in the transformation domain, leading to the proposition of numerous transformation domain fractal features. To effectively leverage the advantages of coherent accumulation and fractal theory, Liu Ningbo et al. combined fast Fourier transform with the fractional Brownian motion model, proposing a target detection method based on frequency domain fractal features [13].

Time–frequency analysis methods, serving as primary tools for analyzing non-stationary random processes, are extensively employed to analyze the non-stationary characteristics of sea clutter. Given the noticeable differences in the normalized time–frequency distributions between sea clutter and target echoes, reference [14] introduced three features, the ridge accumulation, maximum connected region size, and number of connected regions, to characterize this difference, converting the target detection problem into a classification issue in a three-dimensional feature space. An enhanced convex hull learning algorithm was utilized to determine the judgment region, and the effectiveness of the classifier based on three time–frequency features was validated using real data. Reference [15] modeled sea clutter as a compound Gaussian model (CGM) and proposed a block whitening method to suppress sea clutter, further introducing a time–frequency ridge-guided Hough transformation for extracting differential features and utilizing the computed peak values as features for target detection. To increase the utilization rate of echo information, current feature detection methods are progressing toward multidomain, multidimensional, and multifeature directions. Shui Penglang et al. introduced an improved convex hull one-class classifier by establishing a framework for three-feature detection, providing a research idea for multidimensional feature recognition [16].

Polarization information serves as a valuable indicator of the scattering characteristics and physical attributes of echoes. The advent of full-polarization radar technology has spurred increased attention toward echo polarization properties, leading to the introduction of several polarization features for target detection based on the polarization scattering matrix [17]. Guanjian et al. extracted three fundamental features, peak value, centroid frequency, and spectrum width, from the diagonal integral bispectrum. These features are obtained by integrating current frame data with historical frame data, resulting in the accumulation of three cumulative features: cumulative peak, total variation, and

cumulative spectrum width. This cumulative approach effectively enhances the performance of feature detection methods, particularly under conditions necessitating short-term accumulation [18].

Furthermore, various other feature categories have been introduced sequentially for target detection within sea clutter, including graph features [19,20], phase domain [21], and singular spectrum domain features [22].

Despite the substantial and profound developments in radar feature detection methods, certain limitations persist. Practical applications often encounter challenges such as the omission of small targets and a high incidence of false alarms originating from clutter. In multiple fields, weak target detection is gradually gaining attention [23–25]. Common small targets on the marine surface typically encompass anchored small fishing boats, navigational buoys, and similar entities. These objects often possess distinctive structures and physical dimensions compared with larger vessel targets such as cruise ships, cargo ships, and Ro-Ro ships. High-resolution radar systems can provide the one-dimensional range profile features of targets, which reflect the distribution of strong scatterers along the distance. This attribute is critical for distinguishing between small floating targets and larger vessels [26].

However, the efficacy of one-dimensional range profile features is closely tied to observation angles. When radar beams illuminate along the side of a ship, both vessel targets and small floating targets exhibit similar one-dimensional range profile characteristics. This similarity significantly hampers identification performance. Additionally, identifying small floating targets without relying on supplementary information is particularly challenging when using low-resolution radar systems. This difficulty arises from the weak echoes emitted by small floating targets and the fact that large maritime vessel targets typically exhibit substantial radar cross-sectional areas, making them more easily detectable. Fast-moving aerial targets have higher Doppler frequencies, enabling effective radar detection. In contrast, slow-moving or floating entities such as small boats and floating ice have minimal radar cross-sections, resulting in feeble echo energy. This makes it challenging to achieve the minimum detectable signal-to-clutter ratio required by energy domain detection methods. Furthermore, the low velocities of these targets result in smaller Doppler frequencies, which are often overshadowed by the substantial Doppler bandwidth of sea clutter, further complicating target detection in the frequency domain.

By addressing this challenge from the perspective of feature dissimilarity and by thoroughly exploring the distinguishing characteristics between ship targets and small floating targets, it becomes possible to facilitate accurate classification. This classification can aid in determining specific categories, purposes, and threat levels, holding significant implications for both military and civilian applications. Notably, ship targets typically exhibit higher density masses than small floating targets, resulting in relatively stable states under general sea conditions. In contrast, small floating targets frequently oscillate with the waves. Recognizing these differences in fluctuation characteristics through feature detection offers an effective method to distinguish between the two.

It is worth noting that existing feature detection methods typically determine the presence of targets based on whether feature values fall within a predefined decision region, primarily focusing on the distribution of features. However, they often lack in-depth research into target classification. Additionally, the limited utilization of temporal information between features results in inadequate effective feature lengths for the development of target detection and classification methods. In reality, the marine environment is in a continuous state of evolution, leading to dynamically changing backgrounds for sea radar detection. This dynamic nature means that the background information across the entire detection area is not uniform. To achieve robust target detection amidst sea clutter, it becomes necessary to perform a fine-grained dynamic identification of background information across a large detection area. This can be achieved by dividing the detection area into multiple subareas and utilizing temporal information from echo signals. This

approach is of significant importance for target detection and identification, ultimately enhancing the overall performance.

It is not realistic to store radar echoes for a long time during the target recognition stage. If the storage of raw radar echo data is transformed into the storage of feature values, long-term target characteristics can be accumulated. In this context, this paper employs an autoregressive (AR) model to conduct temporal modeling and forecasting of radar echoes within the feature domain, which leverages temporal information from historical frame features as prior knowledge to create new features, thereby extending the effective length of the feature sequence. On this basis, a floating small target classification and identification method based on Doppler spectral centroid time series information is proposed for target recognition. Verification using actual data has indicated that this method achieves a correct classification and identification rate exceeding 92% for both ship targets and small floating targets when using 50 consecutive centroids.

2. Target Discrepancy Feature Extraction

2.1. Extraction of Doppler Spectrum Centroid Sequence

Assume that the maritime radar is conducting surveillance for sea surface targets and receives a pulse string $x(n), n = 1, 2, \dots, N$ of length N on a certain target distance unit, which is the intermediate frequency data collected by ADC and compressed through pulse compression. The pulse string is segmented into non-overlapping short vectors u_i with a length of I as follows:

$$[x(1), x(2), \dots, x(N)]^T = [u_1, u_2, \dots, u_{N/I}]^T \quad (1)$$

Separately calculate the Doppler spectrum of each short vector u_i , and extract the characteristics of the Doppler spectrum centroid. In this chapter, the power spectrum is used as the Doppler spectrum, adopting non-parametric methods in modern signal spectrum analysis for estimating the average and short-time Doppler spectrum. To effectively reduce sidelobes, a windowing treatment is used during estimation.

The Doppler spectrum estimation method is as follows: assume that the length of a single data segment is L ; for the $\phi (\phi = 1, 2, \dots, N/I)$ data segment, the short-time Doppler spectrum estimation value is represented as:

$$\hat{F}_\phi(f_i) = \frac{1}{\sqrt{L\Delta}} \left| \sum_{n=1}^L \omega(n)c^{(\phi)}(n) \exp(-j2\pi f_i Tn) \right| \quad (2)$$

$$\hat{S}_\phi(f_i) = \frac{1}{L\Delta} \left| \sum_{n=1}^L \omega(n)c^{(\phi)}(n) \exp(-j2\pi f_i Tn) \right|^2 \quad (3)$$

$$f_i = \frac{i}{LT}, i = -\frac{L}{2}, \dots, \frac{L}{2} - 1 \quad (4)$$

where ϕ represents the sequence number of the data segment; f_i represents the frequency point; $\hat{F}_\phi(f_i)$ and $\hat{S}_\phi(f_i)$ denote the short-time amplitude spectrum and the short-time power spectrum, respectively; $w(n)$ represents the time-domain window function; T stands for the pulse repetition period (PRP); $c^{(\phi)}(n), n = 1, 2, \dots, L$ denotes the radar echo sequence of the ϕ data segment; and Δ is the power of the window function, represented as:

$$\Delta = \frac{1}{L} \sum_{n=1}^L |\omega(n)|^2 \quad (5)$$

Average the short-time Doppler spectrum along the frequency dimension to obtain the mean Doppler spectrum estimation value, denoted as:

$$\hat{S}(f_i) = \frac{1}{\Phi} \sum_{\phi=1}^{\Phi} \hat{S}_{\phi}(f_i) \quad (6)$$

The Doppler centroid f_C delineates the degree of Doppler shift pertaining to the target, and its estimation method is formulated as:

$$\hat{f}_C(\phi) = \frac{1}{Q(\phi)} \sum_{i=-L/2}^{L/2-1} f_i \hat{S}_{\phi}(f_i) \quad (7)$$

where $Q(\phi)$ illustrates the power level of the short-time Doppler spectrum for the ϕ data segment, defined as:

$$Q(\phi) = \sum_{i=-L/2}^{L/2-1} \hat{S}_{\phi}(f_i) \quad (8)$$

Following the aforementioned methodology, calculate the Doppler spectrum for each short vector u_i individually and extract the features of the Doppler spectrum centroid. Consequently, one can acquire the Doppler spectrum centroid sequence $X_1, X_2 \dots X_{N/I}$ of a certain maritime target.

Experiments were conducted using Datasets A and B to extract the Doppler spectrum centroid sequences of ship targets and buoys (representing floating small targets), enabling the observation of distinctions between these two target categories. A comprehensive introduction to the data is provided in Section 3. The computation of a Doppler spectrum was performed once every 256 pulses, followed by the extraction of centroid features. The resulting typical Doppler spectrum centroid sequences for ship targets and floating small targets (buoys) are visually represented in Figure 1.

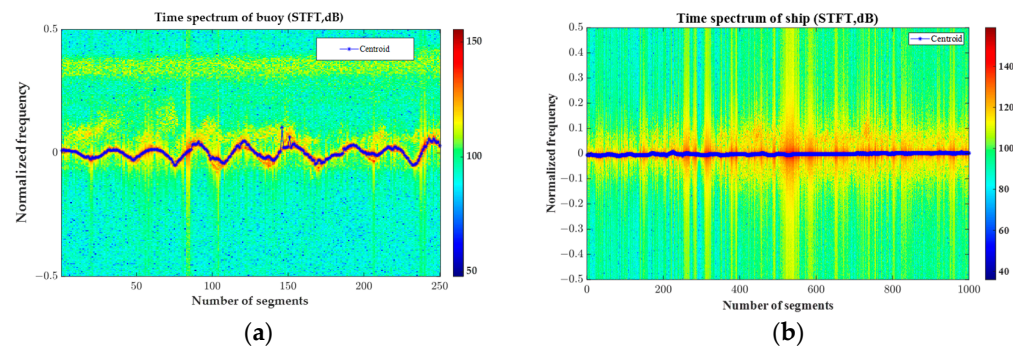


Figure 1. Centroid sequences of the Doppler spectrum of the ship and the buoy: (a) buoy; (b) ship.

It is evident that the Doppler spectrum centroid sequences of ship targets and floating small targets exhibit significantly different patterns of variation. The centroid sequences of ship targets predominantly cluster at approximately 0 Hz and demonstrate relative stability with minimal fluctuations. In stark contrast, the centroid sequences of floating small targets exhibit substantial oscillations, approximating a certain periodicity. Consequently, it is feasible to distinguish between ship targets and floating small targets by analyzing the temporal evolution patterns of these centroid sequences.

2.2. Rectification of Anomalous Values in Centroid Sequences

During radar operations, the presence of random disturbances such as co-frequency interference, noise, and electromagnetic waves of unknown origin often affect the reliability of the signals. These disturbances can induce anomalous values in the extracted Doppler spectrum centroid sequences from the original echo signals. This section introduces a dual-

threshold method to amend the Doppler spectrum centroid sequences, fostering smoother trends and mitigating the effects of these anomalies. The process of employing the dual-threshold method to treat the Doppler spectrum centroid sequences $X_1, X_2 \dots X_{N/I}$ of a specific sea surface target is delineated as follows:

(1) Initialization: Based on the general trend of fluctuations in the centroid sequence, establish two judgment thresholds: standard1 and standard2. When the centroid is dimensioned as a normalized frequency, the value range for standard1 is set between 0.03 and 0.15, and for standard2, it lies within the range of 0.05 to 0.3. For instance, standard1 might be assigned a value of 0.03 and standard2 a value of 0.05.

(2) Processing of X_1 : Determine whether $|X_1 - \text{mean}([X_2, X_3])|$ is less than standard1, where the symbol $\text{mean}(\cdot)$ represents the mean operation and $||$ denotes the absolute value function. If $|X_1 - \text{mean}([X_2, X_3])| < \text{standard1}$, the value X_1 is deemed normal; otherwise, X_1 is deemed an outlier and set to $X_1 = \text{mean}([X_2, X_3])$.

(3) Processing of X_2 : Determine whether $|X_2 - X_1|$ is less than standard1. If $|X_2 - X_1| < \text{standard1}$, then X_2 is classified as a normal value; otherwise, X_2 is identified as an anomalous value and consequently defined as $X_2 = \text{mean}([X_1, X_3])$.

(4) Processing of $X_3, X_4, \dots X_{N/I-1}$: Ascertain whether $X_i - X_{i-1}$ is less than standard1, where $i \in \{3, 4, \dots, N/I - 1\}$. If $|X_i - X_{i-1}| < \text{standard1}$, X_i is categorized as a normal value; otherwise, X_i is deemed an outlier and needs further evaluation if $|X_{i-1} - X_{i+1}|$ is less than standard2. If $|X_{i-1} - X_{i+1}| < \text{standard2}$, X_i is identified as a discontinuous outlier and set to $X_i = \text{mean}([X_{i-1}, X_{i+1}])$; otherwise, it is set to $X_i = \text{mean}([X_{i-2}, X_{i-1}])$.

(5) Processing of $X_{N/I}$: Determine whether $|X_{N/I} - X_{N/I-1}|$ is less than standard1. If $|X_{N/I} - X_{N/I-1}| < \text{standard1}$, then $X_{N/I}$ is classified as a normal value; otherwise, $X_{N/I}$ is identified as an anomalous value and consequently defined as $X_{N/I} = \text{mean}([X_{N/I-1}, X_{N/I-2}])$.

This procedure can likewise be employed to rectify aberrant values in other common feature sequences.

Experimental procedures were conducted using Dataset D. For each batch of 256 pulses, a Doppler spectrum was computed, and centroid features were extracted. Subsequently, the dual-threshold method was applied to correct any anomalies present in the data. In order to demonstrate the effectiveness of the rectification, Figure 2 compares the Doppler spectrum centroid sequences before and after correction. It is evident that the dual-threshold method proposed in this section is capable of achieving noteworthy smoothing effects on anomalous values, effectively addressing the issue of continuous anomaly correction.

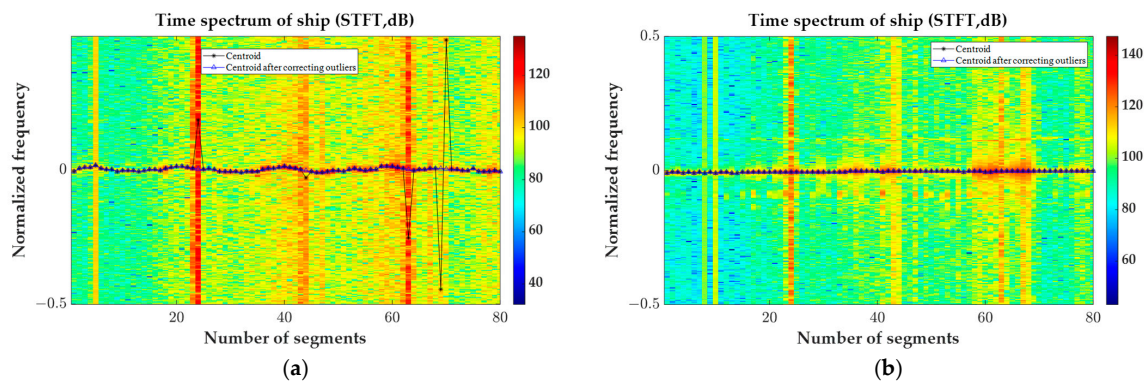


Figure 2. Centroid sequences of the Doppler spectrum of the ship and the buoy before and after anomaly correction: (a) buoy; (b) ship.

2.3. AR Modeling and Secondary Feature Extraction of Centroid Sequences

In this section, the AR modeling of the Doppler spectrum centroid sequence $X_1, X_2, \dots, X_{N/I}$ for a specific marine target is utilized as an illustrative example, delineating the process of conducting AR modeling on the centroid sequences $X_1, X_2, \dots, X_{N/I}$ and extracting the secondary features of the centroids, essentially encapsulating the temporal information

of the centroid sequences. The centroid feature sequences are fitted using a centralized AR(p) model, the results of which are as follows:

$$X_t = c_1 X_{t-1} + \dots + c_p X_{t-p} + \varepsilon_t \quad (9)$$

In this scenario, the model order p is a known quantity, while the model parameters $c = (c_1, c_2, \dots, c_p)^T$ act as parameters awaiting estimation; their moment estimates $\hat{c} = (\hat{c}_1, \hat{c}_2, \dots, \hat{c}_p)^T$ can be calculated utilizing Equation (10):

$$\begin{bmatrix} \hat{\rho}_1 \\ \hat{\rho}_2 \\ \vdots \\ \hat{\rho}_p \end{bmatrix} = \begin{bmatrix} 1 & \hat{\rho}_1 & \dots & \hat{\rho}_{p-1} \\ \hat{\rho}_1 & 1 & \dots & \hat{\rho}_{p-2} \\ \vdots & \vdots & \ddots & \vdots \\ \hat{\rho}_{p-1} & \hat{\rho}_{p-2} & \dots & 1 \end{bmatrix} \begin{bmatrix} \hat{c}_1 \\ \hat{c}_2 \\ \vdots \\ \hat{c}_p \end{bmatrix} \quad (10)$$

Herein, $\hat{\rho}$ represents the estimated value of the autocorrelation coefficient, and Equation (10) is referred to as the parameter estimation method utilizing the Yule–Walker equations. The moment estimate of the white noise variance is depicted as follows:

$$\hat{\sigma}_\varepsilon^2 = \hat{\gamma}_0 - \sum_{j=1}^p \hat{c}_j \hat{\gamma}_j \quad (11)$$

where $\hat{\sigma}_\varepsilon^2$ represents the moment estimate of σ_ε^2 , $\hat{\gamma}_0$ signifies the variance of the centroid feature sequence, and $\hat{\gamma}_j$ represents the autocovariance function with a defined interval j .

Equation (9) presents the AR model fitting results for a certain marine surface target centroid sequence. The order of the AR model p is generally set to 3; consequently, the estimated coefficients of the AR model are denoted as $\hat{c} = (\hat{c}_1, \hat{c}_2, \hat{c}_3)^T$, typically noted as AR(1), AR(2), and AR(3). These constitute the secondary features corresponding to the centroid sequence of a marine surface target, effectively capturing the temporal information embodied in the centroid sequence. Therefore, this chapter adopts this approach for portraying the time series information of the centroid sequence, utilizing it for classification and distinction between ship targets and floating small targets.

Experiments employing Dataset D were conducted, where a Doppler spectrum was computed once every 256 pulses and centroid features were extracted. A sequence of 50 continuous centroids was modeled using the AR(3) model in one instance, depicting the distribution of ship targets and floating small targets (buoys) within the AR coefficient domain of the centroid sequence; as clearly illustrated in Figure 3, the AR coefficient domain of the centroid sequence exhibits commendable separability between two kinds of targets.

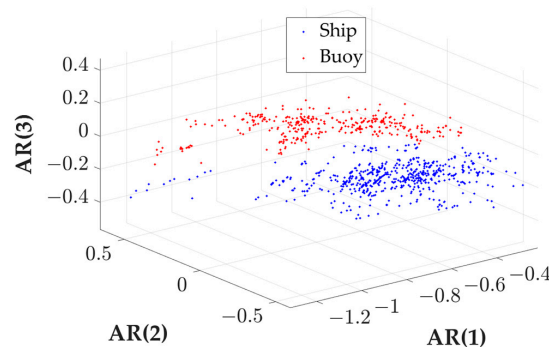


Figure 3. The distribution of ships and buoys in the coefficient domain of the AR model for centroid sequences (Data D).

2.4. Construction of the Classifier and Classification and Identification of Floating Small Targets

After extracting the secondary features AR(1), AR(2), and AR(3) corresponding to the Doppler spectrum centroid sequences of different target echoes, the identification problem essentially translates to a classification problem within a three-dimensional feature space. This chapter situates this problem within the anomaly detection framework and utilizes the convex hull learning algorithm to design a one-class classifier, facilitating the classification and identification between ship targets and floating small targets.

A one-class classifier allows for training solely based on a sample set from one category of data, namely, solely relying on the feature vector set S of ship target echoes processed with labeling. In the three-dimensional feature space, a convex hull encompassing ship target echoes is gradually trained according to a preset probability of erroneous judgment P_f concerning ship targets, thereby effectively mitigating the issue of class imbalance between two types of samples. Adhering to the minimum volume criterion [16], it is prerequisite to apply standard deviation normalization to the set S , preventing the extensive range of variation in the one-dimensional feature value from adversely affecting the classification and identification efficacy of other features. It is presupposed that the training set is represented as:

$$S_0 = [AR(1)_0, AR(2)_0, AR(3)_0] \quad (12)$$

where $AR(1)_0, AR(2)_0, AR(3)_0$ constitute column vectors formed by the secondary features AR(1), AR(2), and AR(3) values of the centroid sequences from a substantial number of ship target units. The length of the vector is denoted as Q . Consequently, the standard deviation of each feature component can be estimated according to Equation (13):

$$\begin{aligned} \sigma_{AR(1)} &= \sqrt{\frac{1}{Q-1} \sum_{q=1}^Q \left(AR(1)_q - \text{mean}(AR(1)_0) \right)^2} \\ \sigma_{AR(2)} &= \sqrt{\frac{1}{Q-1} \sum_{q=1}^Q \left(AR(2)_q - \text{mean}(AR(2)_0) \right)^2} \\ \sigma_{AR(3)} &= \sqrt{\frac{1}{Q-1} \sum_{q=1}^Q \left(AR(3)_q - \text{mean}(AR(3)_0) \right)^2} \end{aligned} \quad (13)$$

where $AR(1)_q, AR(2)_q, AR(3)_q$ denote the q eigenvalues of the feature vector $AR(1)_0, AR(2)_0, AR(3)_0$, respectively, and $\text{mean}(\cdot)$ represents the operation of taking the mean. Consequently, the normalized sample set can be represented as:

$$\begin{aligned} S &= \left[\begin{array}{ccc} AR(1)_0 & AR(2)_0 & AR(3)_0 \\ \sigma_{AR(1)} & \sigma_{AR(2)} & \sigma_{AR(3)} \end{array} \right] \\ &= [AR(1), AR(2), AR(3)] \end{aligned} \quad (14)$$

where AR(1), AR(2), and AR(3) each represent column vectors constituted by the respective normalized features.

Clearly, the samples of ship targets and floating small targets should congregate in distinct regions within the three-dimensional feature space. Consequently, during the training process, the closer that a feature point in the convex hull formed by the ship target samples approaches the aggregation area of the floating small target samples, the higher the likelihood of it being identified as an outlier and being subsequently removed. Thus, the procedure of forming the classifier decision region is delineated as follows:

(1) Initialization: Set the number of feature vectors of the ship target echoes as W , and compute the number of abnormal points of ship targets by $F_{num} = W \cdot P_f$, wherein P denotes the preset erroneous decision probability of ship targets. Let $l = 0$.

(2) Identify the maximum AR (1) feature, as well as the minimum values for AR (2) and AR (3) features within the set S , thereby establishing new spatial vertices $v_0 = [\max(AR(1)), \min(AR(2)), \min(AR(3))]$.

(3) Generate the current data point's convex hull $CH(S)$, with the vertices being denoted as $\{v_1, v_2, \dots, v_r\}$. Count the quantity of feature points falling within the convex hull $CH(S)$ and assign it as n_{all} .

(4) Calculate the Euclidean distance from all feature points to the vertices v_0 , identifying and removing the feature point v_i at the greatest distance.

(5) Construct a new convex hull $CH(S-\{v_i\})$ and then determine the number of feature points located within this new hull, designating it as n_q .

(6) Let $S-\{v_i\} = S, l + n_{all} - n_q = l$.

(7) If $l < F_{num}$, revert to step (2) to proceed with the removal of the next vertex. Otherwise, terminate the removal process and output the final decision region $\Omega = CH(S)$.

Upon the completion of the convex hull single-class classifier training, the collected target echo samples [AR(1), AR(2), AR(3)] are input to achieve classification and identification, adhering to the rules detailed below:

$$\begin{cases} \text{Ship Target if } [AR(1), AR(2), AR(3)] \in \Omega \\ \text{Floating Target if } [AR(1), AR(2), AR(3)] \notin \Omega \end{cases} \quad (15)$$

2.5. Methodology for Floating Small Target Classification and Identification Based on Doppler Spectrum Centroid Temporal Information

Integrating the aforementioned procedures, this chapter proposes a method for floating small target classification and identification grounded on the temporal information of Doppler spectrum centroids. This method delineated in this chapter encompasses two integral components: training and classification identification. Prior to commencing the formal identification work, it is necessary to gather a substantial dataset of ship target echo data, from which the Doppler spectrum centroid sequences are extracted. Following the removal of outliers, a refined centroid sequence is obtained. This sequence is then modeled using the AR (3) framework, facilitating the extraction and normalization of a plethora of secondary features AR (1), AR (2), and AR (3). Ultimately, by employing the convex hull learning algorithm in accordance with a predetermined ship target misjudgment rate, a decision region is established. During the classification and identification phase, the target echo data slated for categorization are processed through the same procedure to acquire normalized secondary feature vectors of the centroid sequence. Classification and identification are achieved by assessing the position of these vectors relative to the established decision region. The block diagram of the method is shown in Figure 4.

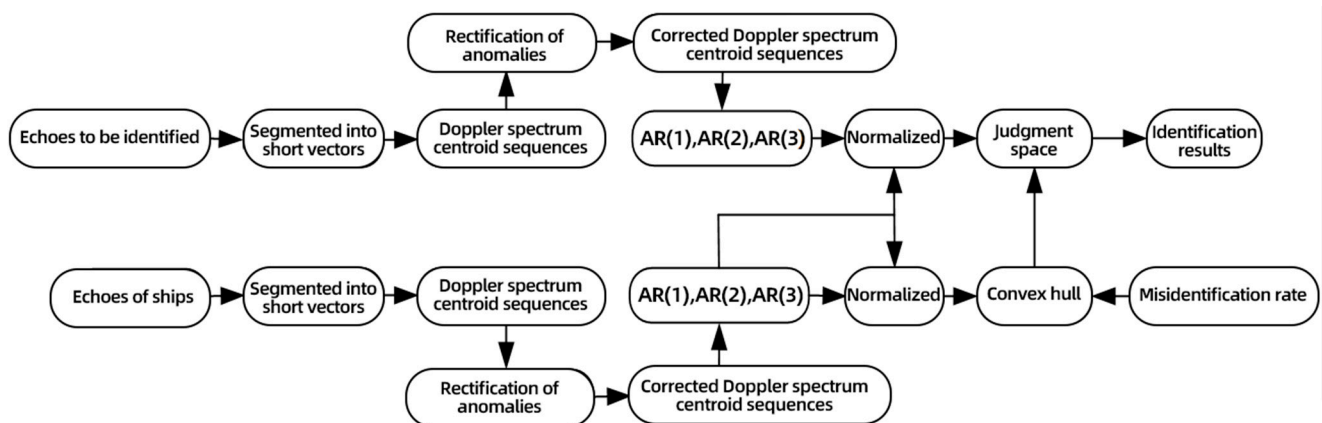


Figure 4. Block diagram of the proposed method.

3. Description of the Experimental Data

In this study, the radar measurement data utilized originate from the self-measured dataset available within the "Radar Marine Detection Data Sharing Program," hosted by the Naval Aeronautical University. This dataset stands as one of the public datasets commonly employed for maritime target detection research in contemporary studies.

Its objective is to conduct phased and batched marine exploration experiments using X-band solid-state phased-array radar. These experiments involve data collection on targets and sea clutter under various marine conditions, resolutions, and grazing angles. Simultaneously, the dataset gathers authentic marine meteorological and hydrological data, along with the actual positions and trajectories of targets. This comprehensive collection of sea clutter measurement data aids in furthering our understanding and suppression of sea clutter characteristics and in the development of target detection and recognition technologies. Relevant data can be obtained from the *Journal of Radars* website (<https://radars.ac.cn/web/data/getData?dataType=DatasetofRadarDetectingSea>, accessed on 1 January 2024).

The radar utilized in the experiments is an X-band solid-state power amplifier surveillance/navigation radar renowned for its high distance resolution and consistent performance. It has the capability of transmitting both single-carrier frequency signals and linear frequency modulation (LFM) signals, meeting the requirements for navigation and coastal surveillance. The dataset primarily encompasses sea clutter and target echo data captured under varying sea states. The radar is located near the first bathing beach in Yantai and is mounted at a height of 80 m. Under different sea state conditions, targets at sea are detected by adjusting the antenna direction, and data on sea clutter and target echoes are collected at various sea state levels. The primary marine targets of interest in this article are floating objects such as navigational buoys and vessels, including fishing boats and passenger ships. During data collection, the radar operated in a staring mode, employing HH polarization with a PRF of approximately 1700 Hz, a distance resolution of approximately 6 m, and a range sampling rate of 60 MHz. Throughout the experimental phase, the test subjects comprised maritime ship targets (large passenger ships) and sea-surface floating objects (channel buoy targets), with the raw echo data being delineated in Figure 5.

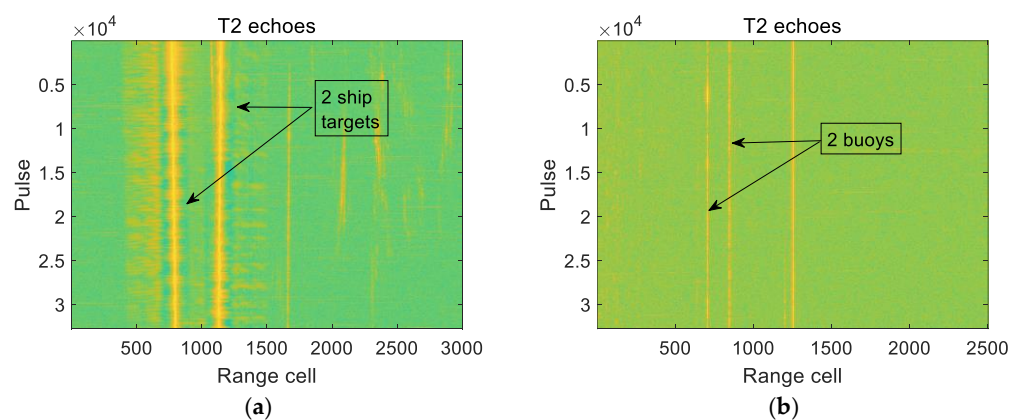


Figure 5. Echoes of two kinds of targets: (a) echoes of ships; (b) echoes of buoys.

The data used in this article encompass four distinct datasets, each of which is detailed in Table 1. For ease of reference, Dataset A is assigned to the dataset labeled as 20221103085038_001_stare_HH_data, Dataset B corresponds to 20221103095714_001_stare_HH_data, Dataset C is denoted as data_2022-08-25 10-43-44_39-41, and Dataset D is identified as data_2022-08-25 10-43-09_38.

Table 1. The introduction to the data collected by our research group.

| Label | File Name | Type of Target |
|-------|----------------------------------|-------------------------------------|
| 1 | 20221103085038_001_stare_HH_data | Data of buoy and sea clutter |
| 2 | 20221103095714_001_stare_HH_data | Data of ship and sea clutter |
| 3 | data_2022-08-25 10-43-44_39-41 | Data of ship, buoy, and sea clutter |
| 4 | data_2022-08-25 10-43-09_38 | Data of ship, buoy, and sea clutter |

4. Performance Analysis

In this section, we employ the self-measured dataset from our research group to test the actual performance of the floating small target classification and identification method proposed in this paper, which is based on the time series information of the Doppler spectrum centroid.

During computations, a Doppler spectrum was calculated with 256 pulses, and centroid features were extracted. A sequence of 50 consecutive centroids was modeled using the AR (3) model once, wherein the AR model coefficients AR (1), AR (2), and AR (3) derived from the modeling of the ship's centroid sequence served as secondary feature samples. When training a convex hull single classifier, the misidentification rate for ship targets was set at 0%, and decisions were made on buoy target samples using an indicative diagram; as illustrated in Figure 6, this achieves a buoy correct identification rate of 100%. It is evident that ships and buoys possess excellent distinguishability in the AR coefficient domain of the centroid sequence, and under certain parameter conditions, the convex hull classifier trained with ship samples can achieve a classification accuracy of 100% for both ships and buoys. Experiments using Data A, Data B, and Data C also attained a favorable distinguishing effect, wherein the results, as displayed in Figures 7 and 8, indicate buoy correct classification identification probabilities of 99.27% for experiments with Data A and B and 92.35% for the experiment with Data C, which are shown in Table 2.

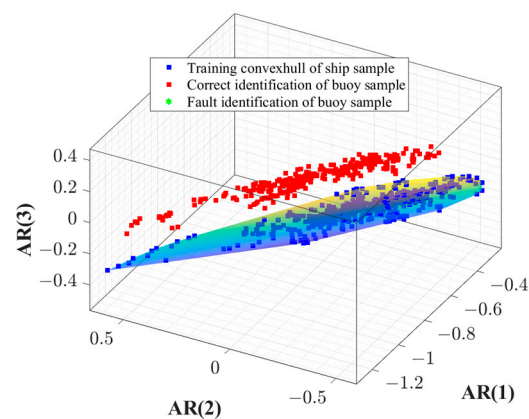


Figure 6. Training and decision diagram of the convex hull classifier (Data 4).

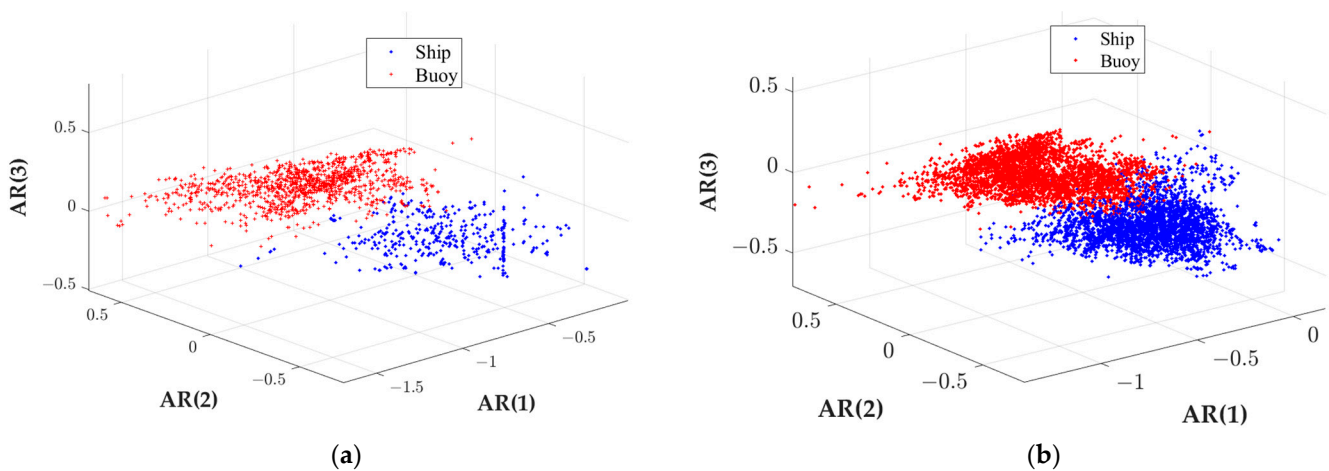


Figure 7. The distribution of ships and buoys in the coefficient domain of the AR model for centroid sequences (she other data): (a) Data A, B; (b) Data C.

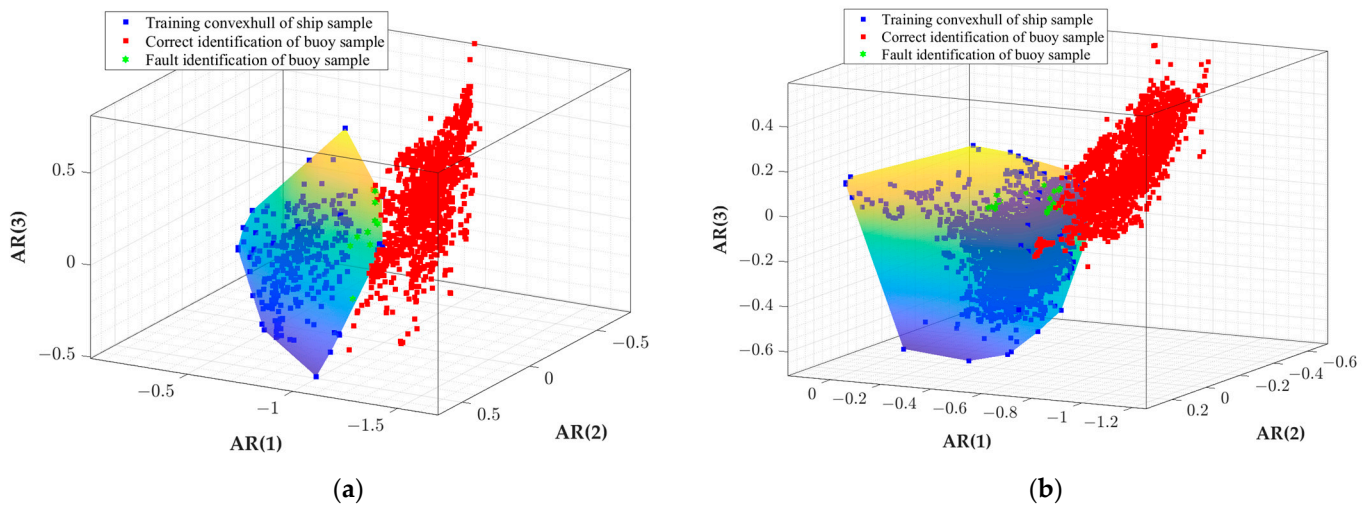


Figure 8. Training and decision diagram of the convex hull classifier (the other data): (a) Data A, B (0% miscalculation rate); (b) Data C (5% miscalculation rate).

Table 2. The recognition rate of measured data.

| | Data A | Data B | Data C | Data D |
|-------------------------|--------|--------|--------|--------|
| Recognition rate | 99.27% | 99.27% | 92.35 | 100% |

It is clear that in the four datasets, with the extraction of the Doppler spectrum centroid feature with 256 pulses and one-time modeling using the AR (3) model for a sequence of 50 continuous centroids, the correct classification identification rate for ship targets and floating small targets (buoys) can exceed 92%.

Utilizing Data D, we altered the number of pulses used for calculating the Doppler spectrum centroid and the number of features (centroid sequence length) used in a single AR modeling to verify the effect of parameter selection on the classification identification results. The results are provided in Table 3, and the outcomes are shown in Figures 9 and 10, exhibiting correct buoy classification identification rates of 80.14% and 100% for pulse numbers of 128 and 256, respectively (the ship target misidentification rate is variable). When the number of pulses for calculating the spectrum centroid was fixed at 256 and the number of features for a single AR model was set to 10, 20, and 50, the results (as depicted in Figures 11 and 12) demonstrate correct buoy classification identification rates of 75.11%, 96.71%, and 100%, respectively.

Table 3. The recognition rate in different conditions.

| Number of Pulses | Number of Features | | |
|------------------|--------------------|--------|--------|
| | 10 | 20 | 50 |
| 128 | 59.6% | 68.5% | 80.14% |
| 256 | 75.11% | 96.71% | 100% |

Generally, both increasing the number of pulses for calculating centroids or augmenting the number of features for AR modeling can effectively enhance the distinguishability between ships and buoys in the AR model coefficient domain of the centroid sequence. In fact, when the observation time is short, in order to display the time–frequency spectrum as much as possible, overlapping data will be used between adjacent data segments when calculating the Doppler frequency of each data segment; let us discuss the impact of the overlapping pulses between adjacent centroids on the distinguishing effect. Utilizing Data D, with a set of 256 pulses for calculating the Doppler spectrum centroid and 128 overlapping pulses used between adjacent centroids in a continuous sequence of 50 centroids

modeled once using the AR (3) model, the ship target misidentification rate was set at 0.2%. The resultant data, illustrated in Figures 13 and 14, reveal a correct buoy classification identification rate of 69.4%. It is apparent that increasing the number of overlapping pulses used for adjacent features significantly reduces the distinguishability between ships and buoys in the centroid sequence’s AR model coefficient domain, primarily due to the alteration of the temporal structure information of the centroid sequence, subsequently affecting the AR modeling coefficients and reducing the distinguishability between ships and buoys.

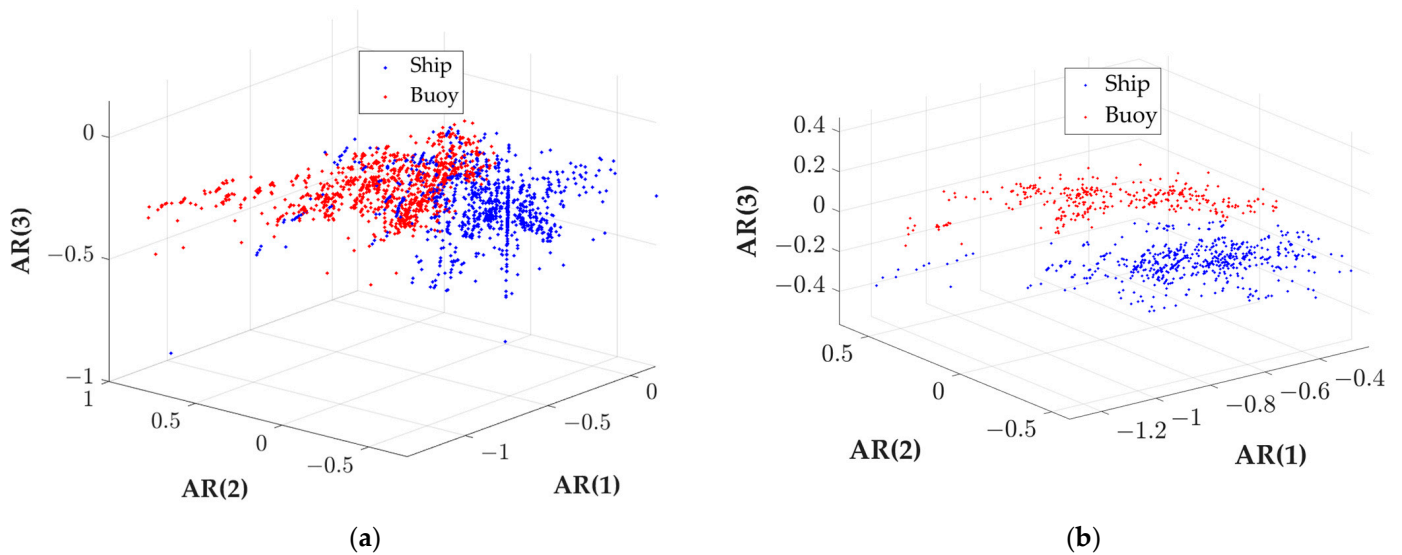


Figure 9. Effect of pulse number on the distribution of ships and buoys in the AR model coefficient domain of the centroid sequence: (a) the number of pulses is 128; (b) the number of pulses is 256.

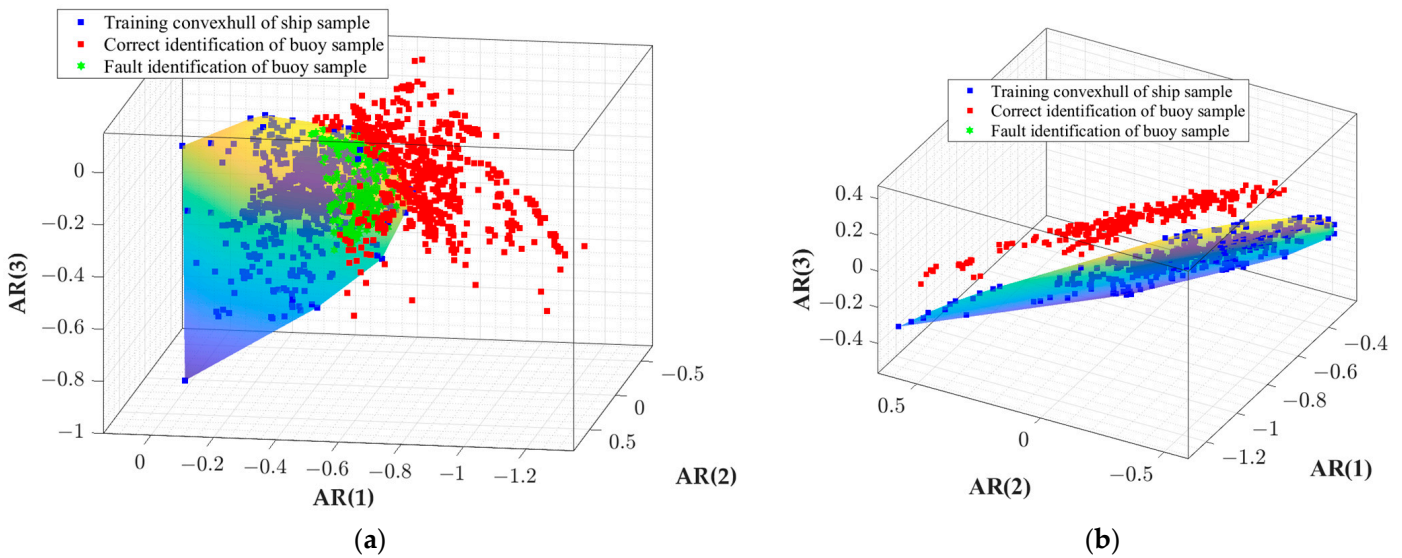


Figure 10. Effect of pulse number on the training and decision effectiveness of the convex hull classifier: (a) the number of pulses is 128 (the miscalculation rate of ship is 15%); (b) the number of pulses is 256 (the miscalculation rate of ship is 0%).

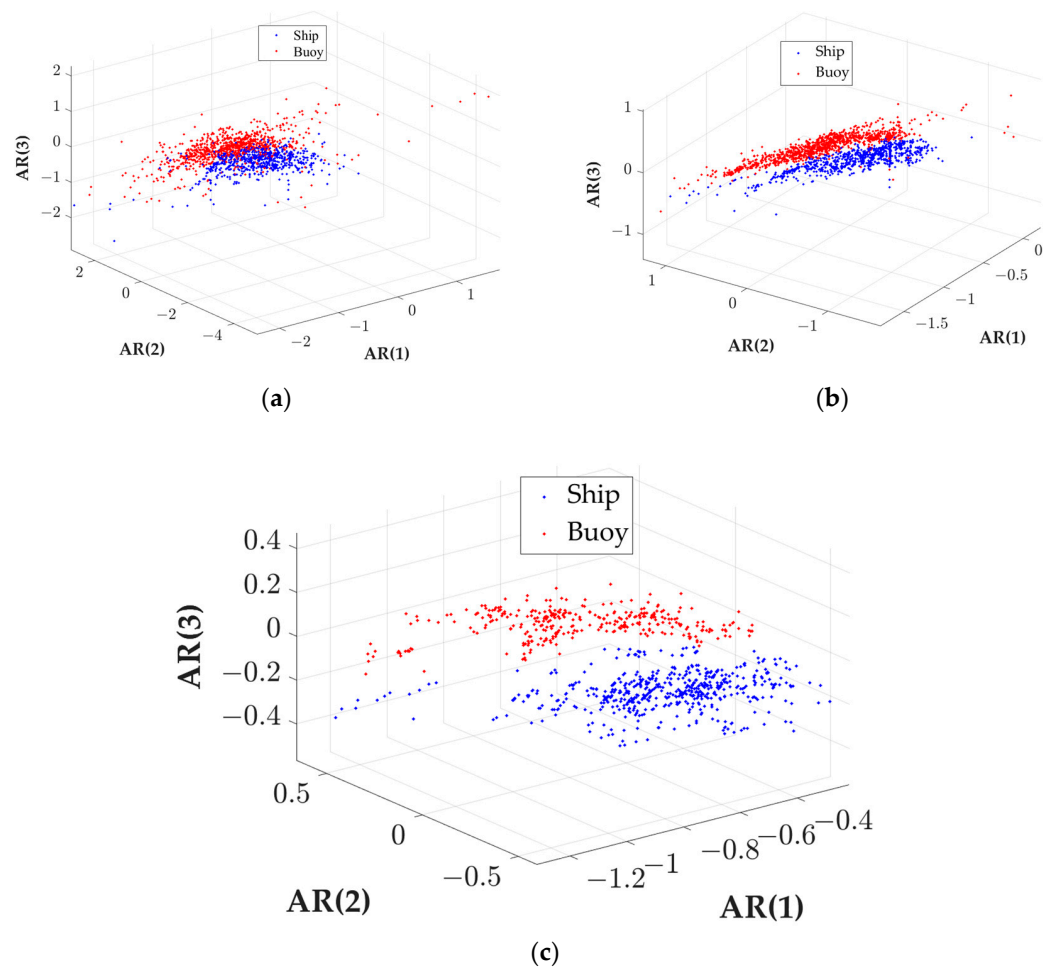


Figure 11. Effect of feature number on the distribution of ships and buoys in the AR model coefficient domain of the centroid sequence: (a) the number of features is 10; (b) the number of features is 20; (c) the number of features is 50.

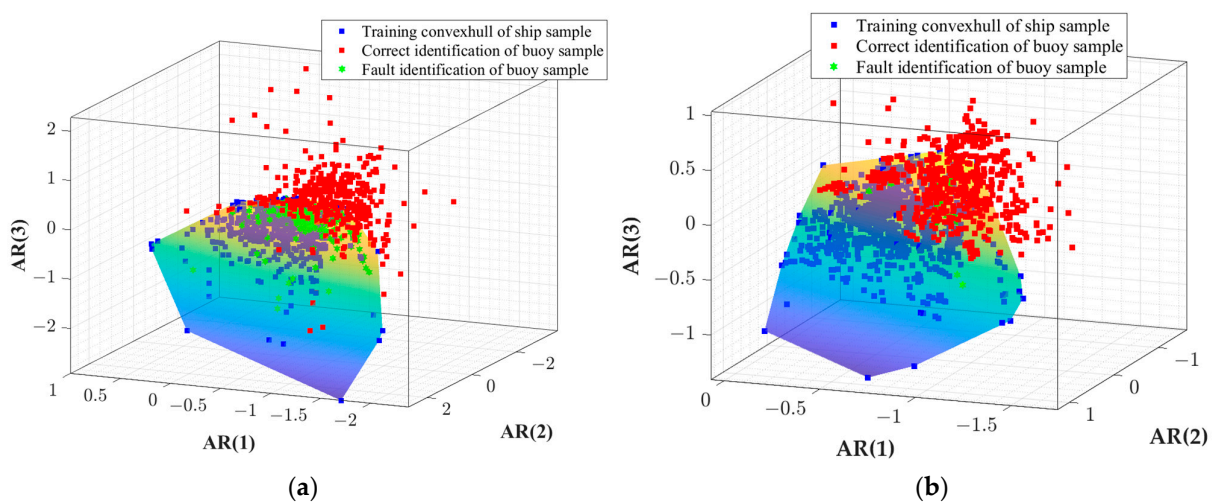


Figure 12. Cont.

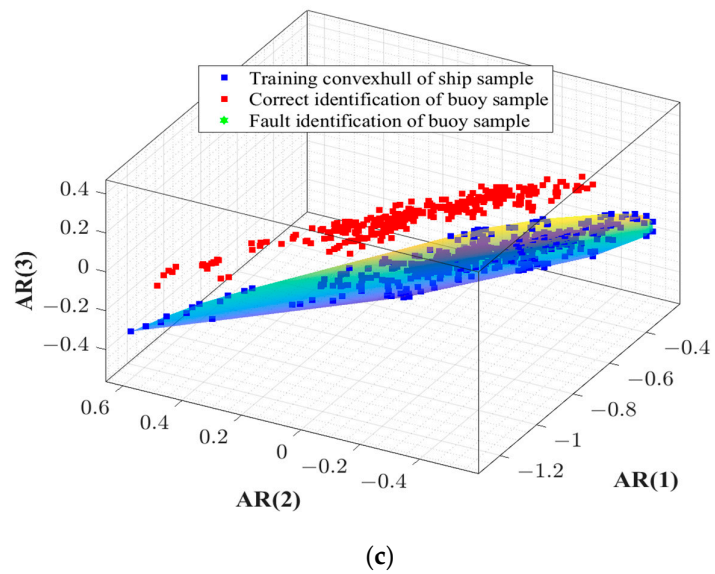


Figure 12. Effect of feature number on the training and decision effectiveness of the convex hull classifier: (a) the number of features is 10 (5% miscalculation rate); (b) the number of features is 20 (0% miscalculation rate); (c) the number of features is 50 (0% miscalculation rate).

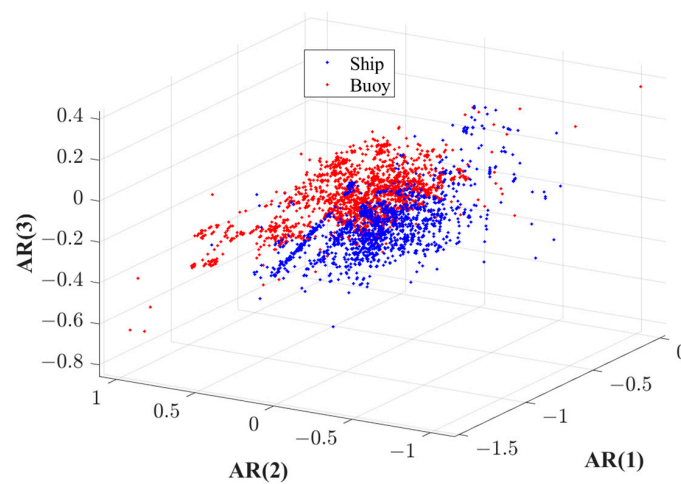


Figure 13. The distribution of ships and buoys in the coefficient domain of the AR model for centroid sequences (the number of overlapped pulses is 128).

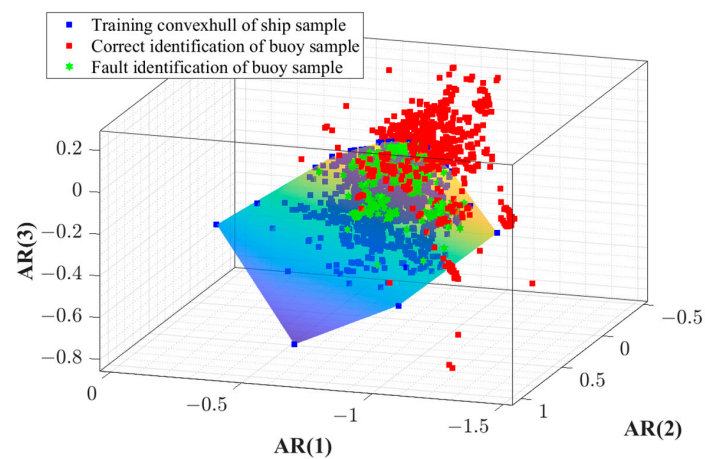


Figure 14. Training and decision diagram of the convex hull classifier (the number of overlapped pulses is 128).

5. Conclusions

This study has introduced a method for the classification and identification of floating small targets, relying on the time series information of Doppler spectrum centroids. We have provided a comprehensive outline of the specific steps involved in this method, which encompass the extraction of Doppler spectrum centroid sequences, the correction of anomalous values in centroid sequences, AR modeling, and the extraction of secondary features from the centroid sequence. Furthermore, we have discussed the construction of classifiers and the subsequent classification and identification of floating small targets.

Utilizing the self-collected data from our research group, we conducted empirical testing of this approach. The analysis of the empirical data reveals that when employing 256 pulses to calculate a Doppler spectrum centroid feature once and utilizing the AR model to model a sequence of 50 consecutive centroid features once, this method can achieve a correct classification and identification rate exceeding 92% for both ship targets and floating small targets. Moreover, increasing the number of pulses used for calculating centroid features or augmenting the number of features in a single AR modeling session can effectively enhance its performance.

Moving forward, we intend to explore other classification methods to further delineate the distinctive features between the two categories of targets. This exploration aims to enhance the accuracy of identification in our ongoing research efforts.

Author Contributions: Data curation, Z.C.; investigation, H.Y. and H.D.; methodology, H.Y. and H.D.; supervision, N.L. and G.W.; writing—original draft, H.Y. and Z.Z.; writing—review and editing, H.Y. and H.D. All authors have read and agreed to the published version of the manuscript.

Funding: This research was funded by the National Natural Science Foundation of China under Grant 62388102, Grant 61871391.

Data Availability Statement: Data are contained within the article.

Conflicts of Interest: The authors declare no conflicts of interest.

References

1. Huang, Y.; Zhang, L.; Li, J.; Chen, Z.; Yang, X. Reweighted tensor factorization method for SAR narrowband and wideband interference mitigation using smoothing multiview tensor model. *IEEE Trans. Geosci. Remote Sens.* **2019**, *58*, 3298–3313. [[CrossRef](#)]
2. Wen, C.; Peng, J.; Zhou, Y. Enhanced Three-Dimensional Joint Domain Localized STAP for Airborne FDA-MIMO Radar Under Dense False-Target Jamming Scenario. *IEEE Sens. J.* **2018**, *18*, 4154–4166. [[CrossRef](#)]
3. Conte, E.; De, M.; Galdi, C. Statistical analysis of real clutter at different range resolutions. *IEEE Trans. Aerosp. Electron. Syst.* **2004**, *40*, 903–918. [[CrossRef](#)]
4. Al-Ashwal, W.A.; Baker, C.J.; Balleri, A.; Griffiths, H.D.; Harmanny, R.; Inggs, M.; Miceli, W.J.; Ritchie, M.; Sandenbergh, J.S.; Stove, A.; et al. Statistical analysis of simultaneous monostatic and bistatic sea clutter at low grazing angles. *IET Electron. Lett.* **2011**, *47*, 621–622. [[CrossRef](#)]
5. Liu, N.; Jiang, X.; Ding, H.; Guan, J. Summary of research on characteristics of radar sea clutter and target detection at high grazing angles. *J. Electron. Inf. Technol.* **2021**, *43*, 2771–2780.
6. Farina, A.; Gini, F.; Greco, M.V.; Verrazzani, L. High resolution sea clutter data: Statistical analysis of recorded live data. *IEE Proc. Radar Sonar Navig.* **1997**, *144*, 121–130. [[CrossRef](#)]
7. Melief, H.W.; Greidanus, H.; Genderen, P.V. Analysis of sea spikes in radar sea clutter data. *IEEE Trans. Geosci. Remote Sens.* **2006**, *44*, 985–993. [[CrossRef](#)]
8. Xu, G.; Xing, M.; Zhang, L.; Liu, Y.; Li, Y. Bayesian Inverse Synthetic Aperture Radar Imaging. *IEEE Geosci. Remote Sens. Lett.* **2011**, *8*, 1150–1154. [[CrossRef](#)]
9. Xu, G.; Zhang, B.; Yu, H.; Chen, J.; Xing, M.; Hong, W. Sparse Synthetic Aperture Radar Imaging from Compressed Sensing and Machine Learning: Theories, Applications and Trends. *IEEE Geosci. Remote Sens. Mag.* **2022**, *10*, 32–69. [[CrossRef](#)]
10. Shui, P.; Xia, X.; Zhang, Y. Sea-Land Segmentation in Maritime Surveillance radars via K-Nearest Neighbor Classifier. *IEEE Trans. Aerosp. Electron. Syst.* **2020**, *56*, 3854–3867. [[CrossRef](#)]
11. Lo, T.; Leung, H.; Litva, J.; Haykin, S. Fractal characterisation of sea-scattered signals and detection of sea-surface targets. *IEE Proc. F Radar Signal Process.* **1993**, *140*, 243–250. [[CrossRef](#)]
12. Kaplan, L.M.; Kuo, C.J. Extending self-similarity for fractional Brownian motion. *IEEE Trans. Signal Process.* **1994**, *42*, 3526–3530. [[CrossRef](#)]

13. Guan, J.; Liu, N.; Huang, Y.; He, Y. Fractal characteristic in frequency domain for target detection within sea clutter. *IET Radar Sonar Navig.* **2012**, *6*, 293–306. [[CrossRef](#)]
14. Chen, X.; Guan, J.; He, Y.; Zhang, J. Detection of low observable moving target in sea clutter via fractal characteristics in fractional Fourier transform domain. *IET Radar Sonar Navig.* **2013**, *7*, 635–651. [[CrossRef](#)]
15. Shi, S.; Shui, P. Sea-surface floating small target detection by one-class classifier in time-frequency feature space. *IEEE Trans. Geosci. Remote Sens.* **2018**, *56*, 6395–6411. [[CrossRef](#)]
16. Shui, P.; Li, D.; Xu, S. Tri-feature-based detection of floating small targets in sea clutter. *IEEE Trans. Aerosp. Electron. Syst.* **2014**, *50*, 1416–1430. [[CrossRef](#)]
17. Xu, S.; Zheng, J.; Pu, J.; Shui, P. Sea-surface floating small target detection based on polarization features. *IEEE Geosci. Remote Sens. Lett.* **2018**, *15*, 1505–1509. [[CrossRef](#)]
18. Guan, J.; Wu, X.; Ding, H.; Liu, N.; Dong, Y.; Zhang, P. A Method for Detecting Small Slow Targets in Sea Surface Based on Diagonal Integrated Bispectrum. *J. Electron. Inf. Technol.* **2022**, *44*, 2449–2460.
19. Yan, K.; Bai, Y.; Wu, H.-C.; Zhang, X. Robust Target Detection Within Sea Clutter Based on Graphs. *IEEE Trans. Geosci. Remote Sens.* **2019**, *57*, 7093–7103. [[CrossRef](#)]
20. Guan, J.; Chen, X.-L.; Huang, Y.; He, Y. Adaptive fractional fourier transform-based detection algorithm for moving target in heavy sea clutter. *IET Radar Sonar Navig.* **2012**, *6*, 389–401. [[CrossRef](#)]
21. Xie, J.; Xu, X. Phase-Feature-Based Detection of Small Targets in Sea Clutter. *IEEE Geosci. Remote Sens. Lett.* **2022**, *19*, 3507405. [[CrossRef](#)]
22. Xiong, G.; Xi, C.; Li, D.; Yu, W. Cross Correlation Singularity Power Spectrum Theory and Application in Radar Target Detection Within Sea Clutters. *IEEE Trans. Geosci. Remote Sens.* **2019**, *57*, 3753–3766. [[CrossRef](#)]
23. Feng, S.; Feng, R.; Wu, D.; Zhao, C.; Li, W.; Tao, R. A Coarse-to-Fine Hyperspectral Target Detection Method Based on Low-Rank Tensor Decomposition. *IEEE Trans. Geosci. Remote Sens.* **2023**, *61*, 5530413. [[CrossRef](#)]
24. Zhang, Y.; Zhang, Y.; Shi, Z.; Fu, R.; Liu, D.; Zhang, Y.; Du, J. Enhanced Cross-Domain Dim and Small Infrared Target Detection via Content-Decoupled Feature Alignment. *IEEE Trans. Geosci. Remote Sens.* **2023**, *61*, 5618416. [[CrossRef](#)]
25. Yan, P.; Hou, R.; Duan, X.; Yue, C.; Wang, X.; Cao, X. STDMA Net: Spatio-Temporal Differential Multiscale Attention Network for Small Moving Infrared Target Detection. *IEEE Trans. Geosci. Remote Sens.* **2023**, *61*, 5602516. [[CrossRef](#)]
26. Guan, J. Summary of marine radar target characteristics. *J. Radars* **2020**, *9*, 674–683.

Disclaimer/Publisher’s Note: The statements, opinions and data contained in all publications are solely those of the individual author(s) and contributor(s) and not of MDPI and/or the editor(s). MDPI and/or the editor(s) disclaim responsibility for any injury to people or property resulting from any ideas, methods, instructions or products referred to in the content.